JCTC Journal of Chemical Theory and Computation

Computational Analysis of Solvent Effects in NMR Spectroscopy

Martin Dračínský* and Petr Bouř*

Institute of Organic Chemistry and Biochemistry, Academy of Sciences, Flemingovo nám. 2, 166 10 Prague, Czech Republic

Abstract: Solvent modeling became a standard part of first principles computations of molecular properties. However, a universal solvent approach is particularly difficult for the nuclear magnetic resonance (NMR) shielding and spin−spin coupling constants that in part result from collective delocalized properties of the solute and the environment. In this work, bulk and specific solvent effects are discussed on experimental and theoretical model systems comprising solvated alanine zwitterion and chloroform molecules. Density functional theory computations performed on larger clusters indicate that standard dielectric continuum solvent models may not be sufficiently accurate. In some cases, more reasonable NMR parameters were obtained by approximation of the solvent with partial atomic charges. Combined cluster/continuum models yielded the most reasonable values of the spectroscopic parameters, provided that they are dynamically averaged. The roles of solvent polarizability, solvent shell structure, and bulk permeability were investigated. NMR shielding values caused by the macroscopic solvent magnetizability exhibited the slowest convergence with respect to the cluster size. For practical computations, however, inclusion of the first solvation sphere provided satisfactory corrections of the vacuum values. The simulations of chloroform chemical shifts and CH *J*-coupling constants were found to be very sensitive to the molecular dynamics model used to generate the cluster geometries. The results show that computationally efficient solvent modeling is possible and can reveal fine details of molecular structure, solvation, and dynamics.

1. Introduction

NMR spectroscopy is extremely sensitive to molecular structure, conformational, and environmental effects.[1−3] Ab initio computations of magnetic shielding[4,5] and indirect spin−spin coupling constants[6] were implemented in many software packages and have become standard tools for a more complete interpretation of the experiment ever since. However, due to the computational cost, these computations are still prohibitive for larger molecular systems. For solution data, it is therefore desirable to find reasonably accurate approximations that would allow accounting for the molecular environment.

The effect of solvent on the NMR parameters is relatively complex. It is difficult to separate the bulk medium effect from more specific interactions.[7] Both the solute and the solvent molecules can also be polarized by electrostatic interactions, make specific bonds involving an electron transfer, and change the conformation in a solution.

Standard polarizable continuum models (PCM) may be used for an estimation of molecular energies and conformations;[8,9] to some extent, they also improve computed vibrational properties.[10] These methods are, however, particularly inaccurate for polar solvents where a directional interaction, typically the hydrogen bond, influences the spectra or conformation.[11−14] Lately, a H⋯π interaction was also detected as an important factor for NMR of aromatic compounds.[15] Similarly, for modeling of properties involving electronically excited states, explicit solvent molecules are a better option.[16−20]

In theoretical modeling of NMR parameters, the PCM methodology certainly improves the vacuum results.[21−23]

* To whom correspondence should be addressed. E-mail: dracinsky@uochb.cas.cz (M.D.), bour@uochb.cas.cz (P.B.).

Nevertheless, the discrete character of real solvents plays an important role also for the NMR spectroscopic response, particularly for polar systems and aqueous solutions.[2,21,24−29]

Previously, we found that the structure of the alanine hydration shell was crucial for understanding the fine chemical shift and spin−spin coupling changes caused by molecular protonation.[24] Also, other studies suggest that the solvent effects cannot be explained on the basis of a simple continuum approach.[26,27] In this study, we analyze a larger set of computational approaches and molecular model systems including both polar and nonpolar compounds to obtain a deeper physical insight into the mechanism of the solvent action. To estimate the bulk effect, the size of the water−alanine clusters was systematically varied, and various solvent models quantitatively were compared in terms of their influence on NMR spectra. The computational modeling is extended by less polar chloroform in various organic solvents. Solvated chloroform also proved to be a convenient model system, as the solute is small, halomethane NMR spectra exhibit a strong dependence on the solvent,[30] and the experiment is relatively straightforward.

Particular attention is paid to the bulk magnetizability that has often been ignored in previous modeling. Yet, it may cause comparatively large differences in chemical shifts with respect to those coming from internal molecular structural changes.[31,32] For a reliable comparison, NMR shifts obtained with different machines or conditions thus have to be corrected for the bulk effects, including factors reflecting shapes of the cells where the sample and the standard were measured.[33]

In this work, we also qualitatively discuss the bulk influence of isotropic and oriented solvent shells on molecular shielding. Other effects including electrostatic and charge-transfer interactions are analyzed in clusters of water and alanine charged forms. The calculated chemical shifts and *J* couplings are compared to the experimental values reported previously.[22] Finally, NMR data for chloroform were measured in various solvents and interpreted on the basis of cluster ab initio computations combined with molecular dynamics (MD) averaging. Although the precision of the Hartree−Fock (HF) and density functional methods is somewhat limited for NMR,[34−36] we are using these approximations because they are computationally efficient and still provide a deep physical insight into the solvation phenomena.

The computed data agree well with observed trends for the NMR parameter changes in various solvents. Both the chemical shift and *J*-coupling values, however, were found unexpectedly strongly dependent on the molecular dynamics model. This suggests that a similar dependence observed for water[24] is quite general, and the NMR parameters also reflect the fine arrangement of other solvent molecules around the solute. Only the combined MD/ab initio strategy is thus able to reliably include the environmental factors and provide means for a more precise NMR determination of molecular structures, dynamics, and interactions with the solvent.

Magnetic Continuum. To better understand the NMR solvation effects, we find it useful to briefly recall the behavior of a magnetic continuum. It has been recognized
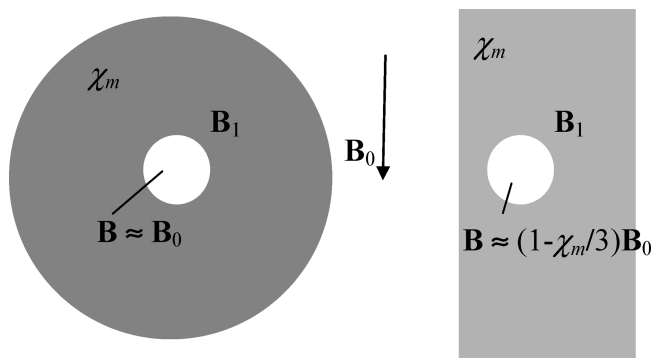

Figure 1. Spherical cavities in a magnetizable sphere and a rod.

that the influence of bulk on measured values of the isotropic magnetic shielding may be very large if compared with the differences originated in fine changes of molecular structure.[31] Modern spectrometers provide various ways of how to compensate these effects, including carefully chosen standards and cell-shape correction factors.[33] Nevertheless, the continuum part must also be considered in the modeling.

Isotropic Continuum Magnetizability. The magnetizability of an isotropic solvent is $\mathbf{M} = (d\mathbf{m})/(dV) = \rho \mathbf{m} N_A / M_w$, where ρ [kg/m^3] is the density, $\mathbf{m}$ [m^{2}A] is the molecular magnetic dipole moment, $N_A = 6.022045 \times 10^{23}$ is Avogadro's number, and M_w [kg/mol] is the molecular weight. The bulk magnetizibility thus can be related to the microscopic dipole $\mathbf{m} = \chi \mathbf{B}$ that is induced by a local magnetic field $\mathbf{B}$ [T]; χ [J/T^2] is the (isotropic) susceptibility.

Using the definition of magnetic polarization, $\mathbf{J} = \mu_0 \mathbf{M} = \chi_m \mathbf{B}$, we can conveniently introduce dimensionless molecular susceptibility as $\chi_m = \mu_0 \rho N_A \chi / M_w$, where $\mu_0 = 4\pi \times 10^{-7}$ [J/(mA^2)] is the vacuum permeability. The local (total) field $\mathbf{B}$ is related to the external field $\mathbf{B}_0$ via

$$\mathbf{B} = (1 + \chi_m)\mathbf{B}_0 = \mu_r \mathbf{B}_0 \tag{1}$$

where μ_r is the relative permeability.[32,37]

In a NMR experiment, an external field of a magnet ($\mathbf{B}_0$) must be differentiated from the actual field in the solvent ($\mathbf{B}_1$) and that acting on a molecule ($\mathbf{B}$). As illustrative examples, consider a cavity in a magnetic "solvent" in the form of a sphere and a long rod (Figure 1). For the sphere, we get a uniform magnetization[31,37] $\mathbf{B}_1 = (1 + \chi_m)/(1 + \chi_m/3)\mathbf{B}_0 \approx (1 + 2\chi_m/3)\mathbf{B}_0$ and $\mathbf{B} = (1 - 2\chi_m/3)\mathbf{B}_1 \approx \mathbf{B}_0$, resulting in a zero bulk shielding. Similarly, for the rod, $\mathbf{B}_1 \approx (1 + \chi_m)\mathbf{B}_0$ and $\mathbf{B} = (1 - \chi_m/3)\mathbf{B}_0$, which corresponds to an NMR shift $\sigma = \chi_m/3$ induced by the solvent. Note that the NMR spectra are typically measured in long tubes that can be well approximated by the rod. Obviously, shapes of generally nonspherical molecules will modify the bulk influence in a more complicated way.

Anisotropic Solvation Shell. The continuum approximation also provides useful qualitative information about a partially oriented solvent layer around a dissolved molecule. In this anisotropic case, the susceptibility of the solvent becomes a position-dependent tensor, $\chi(r)$. An external magnetic field induces in each volume element dV a magnetic dipole of

$$dm = n\chi \cdot B dV \qquad (2)$$

where $n = \rho N_A / M_w$ is a particle density. For small χ, we suppose that $B \approx B_0$. Note the final anisotropic dimensionless shift does not depend on the field. The magnetic field $B(0)$ sensed by a molecule placed at the origin is a sum of the external field B_0 and the contributions from the solvent minute dipoles:

$$B(0) = B_0 + \frac{\mu_0}{4\pi} \int \frac{3rr \cdot dm - r^2 dm}{r^5} \qquad (3)$$

For simplicity, we suppose that the solvent is oriented radially around the solute, with corresponding radial and angular susceptibility components, χ_{rr} and χ_{vv}, that are constant in a hydration shell limited by radii $r_1...r_2$. Then, we can also decompose the induced magnetic moment, $dm = dm_r + dm_v$, where $dm_r = nB_0\chi_{rr}\cos(v)\,dV$ and $dm_v = nB_0\chi_{vv}\sin(v)\,dV$ (Figure 2). Because of the symmetry, only the scalar z-field components need to be considered $B_z(0) = B(0)$, with the ring volume element $dV = 2\pi r^2 \sin(v)\,dvdr$:

$$
\begin{aligned}
B(0) - B_0 &= \frac{\mu_0}{4\pi} \int \frac{3dm_r \cos(v) - dm_z}{r^3} \\
&= \frac{\mu_0}{4\pi} \int \frac{3dm_r \cos(v) - dm_r \cos(v) - dm_v \sin(v)}{r^3} \\
&= \frac{\mu_0 nB_0}{2} \int \frac{2\chi_{rr}\cos^2(v) - \chi_{vv}\sin^2(v)}{r} \sin(v)\,dv\,dr \\
&= \frac{2\mu_0 nB_0}{3}(\chi_{rr} - \chi_{vv})\ln\frac{r_2}{r_1} \qquad (4)
\end{aligned}
$$

Using the dimensionless susceptibilities, we obtain an NMR shift of $\sigma = (2/3)(\chi_{m,rr} - \chi_{m,vv})\ln(r_2/r_1)$. In other words, the orientation of the solvent molecules in the solvation spheres may result in an additional contribution to the solvent shift.

Normally, we can suppose that the oriented solvent layer does not extend too far from the solute. For small molecules, such as alanine and chloroform in the solvents studied below, $r_1 \sim 2$ Å and $r_2 \sim 6$ Å, so that $\ln(r_2/r_1) \sim 1$. Approximating very roughly $\chi_{m,rr} - \chi_{m,vv} \sim \chi_m/2$, we thus get at least a crude estimation of the shift as $\sigma \sim \chi_m/3$. That means that the anisotropic contribution is on the same order as those coming from the bulk. Note that the difference $\chi_{m,rr} - \chi_{m,vv}$
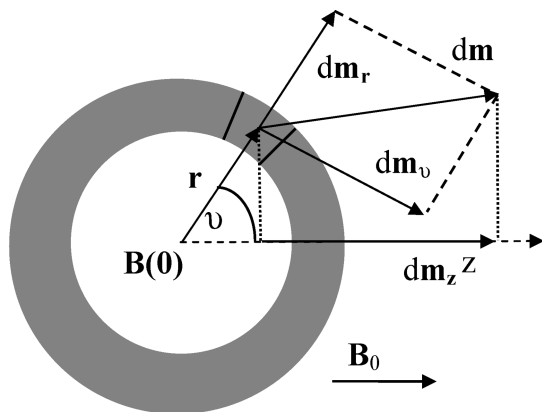

Figure 2. Spherical hydration sphere with a nonisotropic magnetization.

can be both positive and negative, so that the oriented solvent around can either amplify or neutralize the bulk shielding. Indeed, this is consistent with the more quantitative cluster computations presented in this study.

2. The Methods

Experimental Section. The experimental chemical shifts and spin−spin coupling constants obtained for isotopically labeled L-alanine (^{13}C, 98%; ^{15}N, 98%) were reported elsewhere.[22] Three NMR parameter sets for the zwitterionic (AZW, pH = 7), cationic (A$^+$, pH = 2), and anionic (A$^-$, pH = 12) amino acid forms in aqueous (H$_2$O/D$_2$O) mixtures were considered.

Carbon and hydrogen chemical shifts and indirect spin−spin coupling constants in chloroform were measured in six solvents, with the Bruker Avance II-600 spectrometer (600.1 MHz for ^{1}H and 150.9 MHz for ^{13}C). Pure chloroform (CHCl$_3$, 25 μL) was dissolved in a NMR tube with 0.5 mL of deuterated chloroform (CDCl$_3$), benzene, acetonitrile, acetone, methanol, and DMSO. A capillary (∼0.2 mm in diameter) with 30 μL of chloroform was coaxially inserted into the tube as a standard. The ^{1}H and ^{13}C spectra were acquired, and solvent-induced chemical shifts were calculated as a difference between the chemical shifts in the solution and those in the capillary. Alternatively, the spectrometer solvent-correction functions were disabled, and the samples were referenced directly to pure chloroform, which, however, produced nearly the same results. The C−H coupling constants were determined from the distance between ^{13}C satellites in the ^{1}H NMR spectra. We estimate the accuracy of the measured chemical shifts as ∼0.01 and 0.001 ppm for σ_C and σ_H, respectively, and ∼0.2 Hz for the coupling.

Molecular Dynamics. Aqueous alanine (AZW) solvation shells were modeled with the Tinker molecular dynamics (MD) package,[38] using the Amber99 force field[39] that includes the TIP3P[40] water model. One alanine molecule was placed in a (18.56 Å)^3 cubic box, and the molecular dynamics were run using the periodic boundary conditions, NVT ensemble ($T = 295$ K), and a 1 fs integration step. After 10 ps of equilibration, solvent shells were selected from the MD snapshot each 10 ps. Additionally, an arbitrary water force field was used for the same MD runs, where atomic partial charges were set to zero ($q_O = q_H = 0$) and all other TIP3P and Amber99 parameters were unchanged. This choice led to solvation shells where the "water" molecules interacted weakly, which resulted in their different (more irregular) orientations and, consequently, different NMR parameters of alanine.

Alternatively, a larger (37.12 Å^3) cubic periodic box containing one alanine and 1708 water molecules was used in MD with Tinker using the same conditions. After 10 and 15 ps equilibration stages, the geometries were minimized (Amber99/TIP3P), and solvation shells and layers of various sizes specified below (e.g., containing water molecules closer than r_{max} and farther than r_{min} from the solute) were selected with our own Fortran code. Results obtained with the two MD snapshots were very similar with respect to the size-convergence behavior, and thus only the 10 ps case is shown.

Computational Analysis of Solvent Effects

J. Chem. Theory Comput., Vol. 6, No. 1, 2010 **291**

Table 1. Calculated and Experimental Solvent Magnetic Susceptibilities

solvent	$\chi^{a,b}$	$\chi^{a,c}$	ρ^d	$\chi_m^{c,e}$	$\chi_m^{exptl\ f}$
water	−220	−235	1.00	−9.9	−8.91
methanol	−355	−364	0.79	−6.8	−6.91
chloroform	−991	−1087	1.49	−10.3	−9.19
acetone	−555	−569	0.78	−5.8	−5.67
DMSO	−765	−778	1.10	−8.3	−7.81
benzene	−930	−931	0.87	−7.9	−
acetonitrile	−406	−419	0.79	−6.1	−6.57

^{a} Molecular magnetic susceptibility, in 10^{-30} J T^{-2}. ^{b} B3LYP/6-31G** calculation. ^{c} B3LYP/6-311++G** calculation. ^{d} Density (g/mL) used. ^{e} Relative bulk magnetic susceptibility, in parts per million. ^{f} Ref 33, in parts per million.

To obtain a deeper physical insight into the influence of the solvent on the NMR calculations, we also used four alanine/water clusters that were previously obtained with the Car−Parrinello molecular dynamics (CPMD).[24] The more demanding CPMD simulation did not enable the inclusion of larger clusters, but water distribution obtained by this method is more realistic and provides NMR data more comparable with experimental results than from the classical MD.[24,41] The ab initio dynamics were based on the BLYP[42] functional and Vanderbilt[43] ultrasoft pseudopotentials; an energy cutoff of 25 Ry and a 4 au integration time step were used under temperatures of 300 K. A shorter time step than for the classical dynamics had to be used to allow for the relaxation of the electronic wave function, which is performed on the fly in CPMD.[44] Four cluster sets were selected, at 1.5, 5.0, 5.5, and 10 ps. Our own scripts were used to reduce the number of water molecules to for to nine so that hydrogen-bonded water molecules closer than 3.6 Å to the solute were retained only.[24] The distance of 3.6 Å allows to fully include the first hydration sphere. These "smaller" clusters were used by default. Similarly, larger clusters were made where all water molecules up to 4.5 Å were retained. In the resultant clusters, the alanine geometry was optimized ab initio with a fixed geometry of the water molecules.

Similarly as for the alanine, chloroform solvation, and solvent dependence of the NMR parameters was investigated with the aid of clusters obtained by the Tinker[38] MD and MM3[45] force field. Periodic cubic boxes of chloroform (sized 35.98 Å) and chloroform in the benzene (35.99 Å), methanol (36.00 Å), acetone (36.01 Å), acetonitrile (36.01 Å), and dimethylsulfoxide (CH$_3$SOCH$_3$, DMSO, 35.52 Å) solvents were subjected to equilibration MD runs for 10 ps. Both NVT and NpT thermodynamical ensembles were investigated at a temperature of 295 K and a pressure of 1 atm. For the NpT simulations, the solvent could more easily relax and orient itself around the solute than for NVT ensembles, but equilibrated solvent NpT densities were lower (by ∼25%) than the experimental ones (Table 1) due to force field inaccuracies. A total of 10 MD snapshots at 10 ps intervals were used to generate solvated chloroform molecules where all solvent molecules closer than 9 Å were retained. On average, the clusters with central solvated chloroform contained 44 MeOH, 20 CHCl$_3$, 18 acetone, 33 acetonitrile, 14 C$_6$H$_6$, and 18 DMSO molecules. Resultant clusters were subjected to constrained normal mode optimization of the geometry.[46,47] Vibrational modes with wavenumbers within

−300 to + 300 cm^{-1} were fixed (imaginary frequencies were considered as negative), so that the MD solvent distribution could be approximately conserved, but molecular geometry, particularly the bond lengths and angles, could relax at a higher, BPW91[48]/6-31G** level.

NMR Computations and Solvent Models. The NMR parameters were computed ab initio for simplified solvent models that included (1) solute in the gas phase, (2) solvent molecules explicitly included in the CPMD and MD clusters, (3) CPMD clusters surrounded by a polarizable PCM continuum,[49] (4) clusters where the solvent molecules were replaced by TIP3P[40] partial atomic charges ($q_O = -0.834$, $q_H = 0.417$, for water) and electrostatically fitted charges[50] from Gaussian (for the nonaqueous solvents), (5) using the same point charges surrounded by a PCM continuum, and (6) the solute in plain PCM. To investigate the "pure" polarizability effects (7), water molecules were also replaced by neon atoms placed at the water oxygen positions. Finally, (8) the nucleus-independent chemical shift (NICS)[32,51] was calculated for the CPMD and MD clusters where the solute molecule was removed from the cluster and only its solvation shell remained. For the ghost atoms in NICS, the *J* coupling was also calculated and related to the nuclear momenta of the substituted atoms.

Molecular magnetic susceptibilities, NMR isotropic shielding, and indirect spin−spin coupling (*J* coupling) were calculated with the Gaussian program.[52] All four *J*-coupling terms (Fermi-contact, spin-dipolar, diamagnetic, and paramagnetic spin−orbital)[6] were included. The hybrid B3LYP[42] functional with 6-31G** and 6-311++G** Pople-type basis sets was used for the susceptibilities. The default GIAO orbitals were used[4] in all calculations. Some alanine NMR parameters were obtained for CPMD clusters from ref 24 at the B3LYP/6-311++G** level. The Hartree−Fock (HF)/6-31G approximation was used for the larger (MD) clusters of alanine and water, because the DFT methods (B3LYP and BPW91) exhibited numerical instabilities for very large clusters. NMR shielding and *J* coupling in chloroform solvated by the organic solvents were calculated with the B3LYP and BPW91 functionals and 6-31G** basis set. Other basis sets were also tried (IGLOII and IGLOIII, not shown) but did not bring new insight. The accuracy of NMR properties is known to be significantly dependent on the quality of the basis set;[2] however, in this study, similarly as in previous works,[22,24,53] other limitations, such as the accuracy of the DFT methods, appear more important.

3. Results and Discussion

The Bulk Influence. The isotropic shielding caused by the bulk environment (cf. eq 1) can often be suppressed by suitable experimental conditions.[33] Its detailed modeling at the atomic level is beyond the main scope of this study; nevertheless, we can estimate at least its approximate magnitude from Table 1, where calculated (B3LYP/6-31G** and B3LYP/6-311++G**) dimensionless susceptibilities, χ_m, are compared to the experimental values from ref 33. Note that for a spherical cavity in a rod (Figure 1) the bulk shielding would be $\sigma = \chi_m/3$ and so forth. Such a geometry model is appropriate for most NMR experiments with
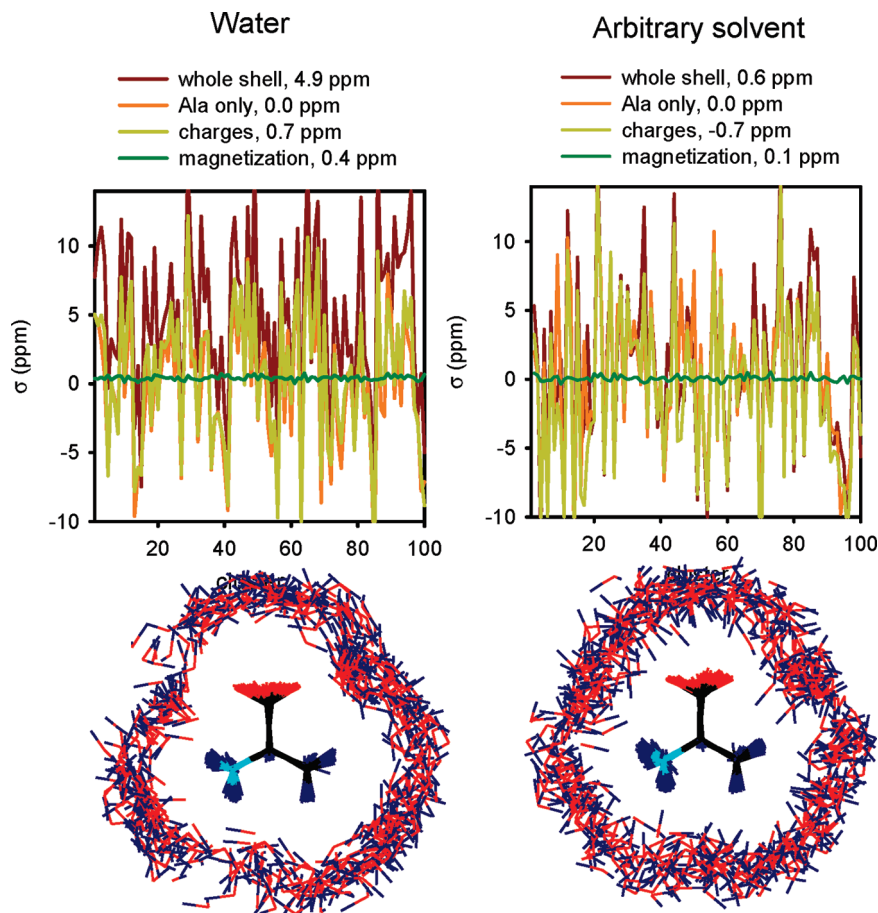
Figure 3. Example of water (left) and a less-oriented (right, "water" without charges) alanine solvation shell (3−4 Å). For 100 MD clusters, calculated (HF/6-31G) average and immediate nitrogen chemical shift changes (σ) are plotted as caused by the shell (maroon), alanine distorsions only (orange, the average is taken as a reference), partial charges mimicking the water molecules (yellow, $q_H = 0.42$, $q_O = -0.84$), and the magnetic NICS contribution (green). In the bottom, cross-sections 1-Å-thick through the overlapped hydration shells are plotted.

approximately spherical molecules measured in a prolonged (rotating) capillary. As apparent from the table, the ab initio computations with the 6-31G** and 6-311++G** basis sets produced similar results, and the calculated values very well (within 2−12%) agreed with the experiment. Clearly, the bulk magnetizability can cause chemical shift differences of several parts per million between various solvents, and as such it cannot be neglected in precise modeling.

The Solvent Orientation Effect. We have seen (eq 4) that oriented solvent can specifically contribute to the bulk influence, depending on the fine structure and extent of the solute hydration sphere. For oriented solvents and crystals, the derived logarithmic dependence of the shielding contribution on the distance means that clusters of limited sizes are not relevant for the theoretical modeling. Fortunately, for usual solvents, the solvent ordering is restricted to the first hydration sphere and thus better susceptible to modeling at the atomic level. On the example of a hydrated alanine zwitterion (Figure 3), we can follow both immediate and average hydration effects on the isotropic shielding of nitrogen. The behavior of other atomic shifts was similar.

In the solvent shell selected in Figure 3, immediate solvent configurations disperse the nitrogen shift within a large interval, ∼−10 to +13 ppm if compared to the reference vacuum value. After averaging, the oriented aqueous solvent produces a significantly different average shift of 4.9 ppm (left of Figure 3) than the chargeless artificial "water" model (0.6 ppm, Figure 3, right). A replacement of the water atoms by atomic partial charges (yellow curves) produces qualitatively similar dispersion to that of the explicit model, but corresponding average shift values obtained with the normal and chargeless water models (0.7 and −0.7 ppm, respectively) are quite different again. We can also see that the water magnetizability itself (green line) makes only a tiny contribution to the overall solvent effect. Its dispersion is also very small. Nevertheless, its average cannot be ignored for precise modeling. The more oriented case provides a value (0.4 ppm) that is significantly larger than that for the less-oriented model (0.1 ppm). This computational exercise is consistent with many cluster NMR studies,[24,26,27] indicating that the shift dispersion caused by the solvent configuration is huge, and a relatively large amount of MD configurations has to be taken for converged results.

Cluster Size Convergence. The cluster size convergence of the shielding caused by the bulk magnetazibility is rather slow (cf. eqs 3 and 4). It also strongly depends on the cluster shape (cf. Figures 1 and 2). However, this contribution is relatively minor (cf. Figure 3, green lines), and for practical computations, the principal solvent effects on NMR shielding can be reasonably approximated by a finite cluster of the
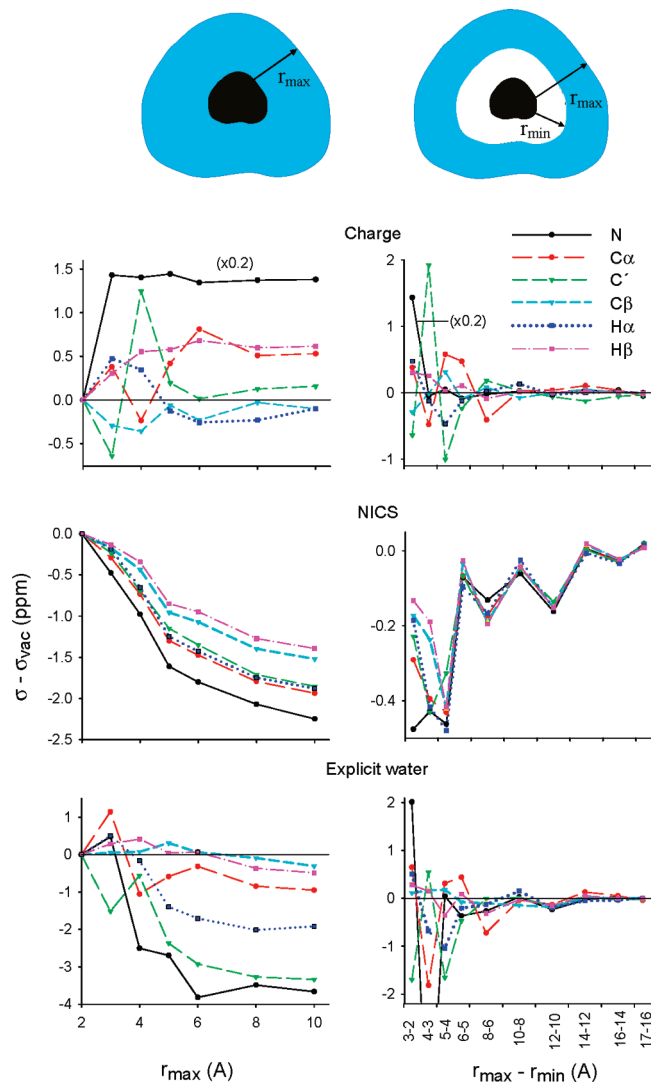
Computational Analysis of Solvent Effects

J. Chem. Theory Comput., Vol. 6, No. 1, 2010 **293**

Figure 4. Calculated (HF/6-31G) dependence of chemical shifts in the alanine zwitterion on the hydration shell radius (left) and the chemical shifts obtained with variously sized shell layers (right). A randomly selected MD cluster was used; the shifts are referenced to alanine in a vacuum.

solvent molecules around the solute. Indeed, as shown in Figure 4 (left) where alanine zwitterion shielding changes with respect to the vacuum caused by variously sized solvation shells are plotted, solvation shells of $\sim 8-10$ Å seem to provide reasonably converged results. The contributions obtained with the partial atomic charges and NICS are plotted separately in Figure 4. The size of the full shells with explicit water molecules is limited to $r_{max} \leq 10$ Å because of the computer time and memory limits. For example, the HF/6-31G NMR computation took 11 min for the 4 Å sphere (14 waters, 250 basis functions, about 50 MB of memory needed) and 7 h for the 8 Å sphere (100 waters, 1368 b.f., ~ 1 GB) if related to one 2.6 GHz AMD processor. Nevertheless, on the basis of previous analysis in Figure 3, we can suppose that averaging of the water orientations in the shell layers will further limit the influence of a distant hydration. Most of the shielding changes occur up to ~ 5 Å thickness (Figure 4); nevertheless, for example, the chemical shift of the hydrophobic C^α carbon is still notably influenced by solute molecules at a distance of ~ 6 Å from the solute.

A pure electrostatic influence of the solvent simulated by the partial atomic charges fades relatively quickly, at $r_{max} \sim 5$ Å. This suggests that other effects are important for the total solvent-induced shift, such as making the hydrogen bonds associated with partial electronic transfer and polarization of the solvent by the solute, also neglected in the charge model. Particularly, the NICS "bulk" magnetizability (the middle row of graphs in Figure 4) converges very slowly. In accord with the above-mentioned discussion, the NICS values are similar for all atoms ($\sim 1.3-2.2$ ppm for the 10 Å shell) and qualitatively correspond to the shielding in a spherical aqueous cavity ($\chi_m/3 \sim 3$ ppm, cf. Table 1).

An alternate view is provided by the contributions from variously distant hydration layers plotted at the right-hand side of Figure 4. This approach allowed for a slightly larger distances ($r_{max} \leq 17$ Å) because the layers contained fewer water molecules than the full shells. In addition to the dependencies discussed for the full shells, we see that the contributions from individual layers of similar thickness diminish much faster with the maximum distance than for the full shells at the left-hand side of the figure, although the layers still contain a number of water molecules increasing as $\sim r^2$. Their decreasing influence on the chemical shifts is not monotonic, but it is modulated by actual water distribution/orientation in the layer. This is consistent with the shift dispersion caused by the solvent observed for a fixed-sized shell in Figure 3.

A relatively large basis set superposition error was found for the smallest alanine/water clusters (not shown), especially for the nitrogen shift, where it caused variations up to 1.5 ppm. Therefore, a fixed number of basis functions corresponding to all water molecules and $r_{max} = 4$ Å was kept in clusters smaller than this value.

Hydration Shell Additivity. Because the hydration layers influence the solute shifts in a relatively complex way, their effect is additive only roughly. This is demonstrated in Figure 5 for a $5-6$ Å layer obtained from MD (Amber99/Tinker). For example, the addition of a layer-1-Å thick to the 5 Å shell does not noticeably change the original nitrogen σ_{xx} shielding density (top of Figure 5). In the bottom of Figure 5, in a more quantitative way, the approximate additivity is illustrated on individual AZW chemical shifts (with respect to the vacuum). Indeed, the shifts obtained with the $5-6$ Å solvent layer follow the differences of shifts obtained with the complete 6 Å and 5 Å clusters. Other solvent shells (e.g., $3-4$, $4-5$ Å, not shown) behaved similarly. In the present example, a considerable deviation from additivity appears, namely, for the polar nitrogen atom. Nevertheless, on the basis of these observations, we can conclude that the NMR solvent effect is primarily caused by through-space electric and magnetic "additive" interactions rather than an electron transfer and similar solvent-mediated effects.

Solvent Contributions to NMR Shielding. Although we cannot separate individual mechanisms taking part in the solvent effect, they can be partially deduced from the comparison of various solvation models. In Figure 6, we compare isotropic shielding (relative to vacuum) of selected nuclei in the alanine zwitterion as obtained with several solvent approximations. The results for the other two A^+
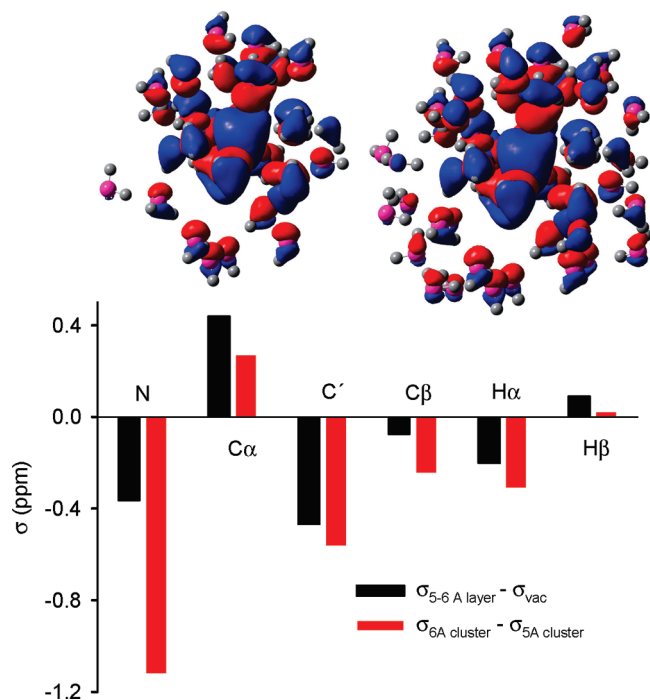
Figure 5. (Top) Nuclear shielding density (HF/6-31G, σ_{xx} isovalues at 0.02 au) calculated for the nitrogen atom in AZW surrounded by 5 Å (left) and 6 Å (right) hydration spheres. (Bottom) Difference of the chemical shifts obtained with the full 5 Å and 6 Å hydration shells (red, and the shift changes caused by the 5−6 Å layer only (black).
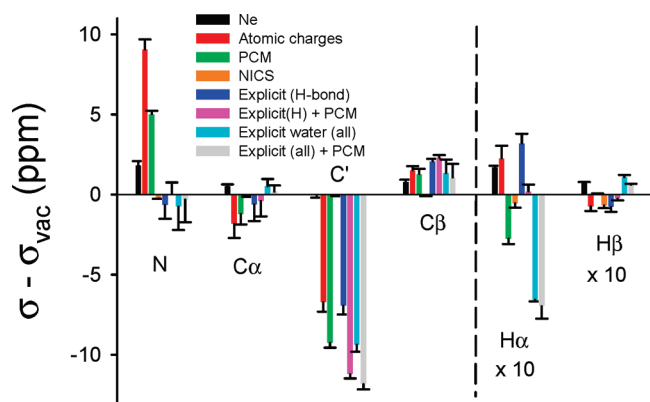

Figure 6. AZW chemical shifts calculated (B3LYP/6-311++G**) with various solvent models: (black) water molecules replaced by neon atoms and BSSE-corrected, (red) water molecules replaced by TIP3P atomic partial charges, (green) plain PCM, (yellow) the NICS contribution, (blue) explicit hydrogen-bond water clusters, (magenta) the clusters surrounded by PCM dielectric, (aqua and gray) larger clusters where also non-hydrogen-bonded water molecules were included, without and with the PCM environment. Results obtained as an average of four (two for the last two models) CPMD clusters are shown.

and A⁻ charged forms were similar to AZW and are not shown. For example, replacing the solvent by neon atoms placed at the water oxygen positions already causes significant chemical shift changes. This effect is relatively large for the hydrogen nuclei. It does not correspond well to the last, presumably most accurate, large cluster/PCM model. Nevertheless, the "plain polarization", in this case that of

the electrically neutral Ne atoms, significantly contributes to the NMR solvent effect. It should be noted that neon polarizability is a fraction (∼20%) of the aqueous one; modeling with other rare gas species, however, was problematic because of their large van der Waals radii. The neon radius, on the other hand, is very close to that of oxygen.

The C′ and C^{β} shifts induced by the atomic partial charges (cf. Figure 6) copy the benchmark results (the last model in Figure 6) much more faithfully. The charge approximation, however, is fully inadequate for the nitrogen shielding, differing by ∼10 ppm from the more advanced approximations. More importantly, the widely used PCM model (green bars in Figure 6) also fails for the nitrogen. Clearly, for accurate calculation of NMR parameters, explicit water molecules are needed to model the hydrogen bonding and electron transfer associated with the solvation of the NH_3^+ group. Similarly, computations of amide electronic excitations are required to include the water molecules explicitly.[18] On the other hand, the charge approximation could be used for modeling of the vibrational amide properties.[12,54]

The PCM model also gives rather erratic results for H^{α} and H^{β} shifts. Even the models comprising H-bond waters in smaller clusters (blue and magenta bars in Figure 6) fail in this case. Clearly, for the aliphatic hydrogen magnetic shielding, the inclusion of all water molecules around the solute is more important than for the heavy atoms. This can be understood since H^{α} and H^{β} do not form hydrogen bonds that were used for the water selection in the smaller clusters. Nevertheless, the addition of the PCM model seems to be still important for the largest clusters, where the longer-range polarization forces can significantly modulate the NMR shielding. It should be noted that experimental chemical shift variations for hydrogen, for example, in proteins, are much smaller than those for heavy atoms, which corresponds to the smaller absolute values for shifts comprising the H^{α} and H^{β} atoms (cf. the *y* scale in Figure 6). Relative chemical shift variations for hydrogen and heavy atoms are dependent on the chosen reference (standard) and can generally be comparable.

The NICS contributions caused by the water magnetization only seem to be negligible for the heavy atoms. Presumably, they are overpowered by the currents magnetically induced inside the alanine molecule. However, they are very important for the hydrogen atoms, which are surrounded by a sparser electron density and clearly more susceptible to the magnetic currents induced in the solvent. Note that the size of the NICS effect is about the same for all atoms, similar to the bulk effect discussed before, which also makes it more important for the hydrogens where the absolute shifts are small.

These findings are supported by the data in Table 2, where the calculated chemical shifts of A⁻ and A⁺ (with respect to AZW) are compared to the experiment. In particular, although the point charge model was not adequate for the nitrogen shielding, it provides on average better results than PCM. The NICS bulk magnetic contribution is negligibly small, except for the hydrogen shielding of A⁻. As expected, the largest clusters surrounded by the PCM dielectric lead to the most accurate results.

Table 2. Chemical Shifts (ppm) in the Charged A$^+$ and A$^-$ Forms Referenced to the Corresponding Nuclei in AZW as Calculated (B3LYP/6-311++G**) with Different Solvent Models[a]

	vacuum	PCM[b]	point charge	NICS	charge+PCM	cluster	cluster+PCM	exptl[b]
				$\sigma(A^+) - \sigma(AZW)$				
N	−3.54	−3.32	−2.84	0.02	−3.89	−1.79	−1.82	−2.20
C′	1.79	−1.04	−1.17	0.05	−1.24	−1.42	−1.80	−1.77
C$^\alpha$	3.12	−1.38	−0.44	0.09	−1.53	−0.23	−1.86	−3.11
C$^\beta$	−3.09	−2.60	−1.68	0.03	−2.42	−0.87	−1.30	−0.83
H$^\alpha$	0.67	0.75	0.65	0.08	0.70	0.62	0.75	0.37
H$^\beta$	0.51	0.25	0.32	0.02	0.27	0.28	0.22	0.08
$\Delta\sigma^c$	2.35	0.98	0.88		0.99	0.69	0.44	0.00
				$\sigma(A^-) - \sigma(AZW)$				
N	−12.97	−11.62	−8.28	−0.23	−10.65	−8.96	−8.34	−6.60
C′	2.48	0.98	0.92	−0.18	1.03	0.47	0.77	0.93
C$^\alpha$	14.96	12.71	12.87	−0.08	12.57	11.53	10.28	8.94
C$^\beta$	3.03	4.08	3.73	−0.15	4.49	3.03	3.11	4.25
H$^\alpha$	−0.97	−0.90	−0.73	−0.22	−0.88	−0.56	−0.63	−0.48
H$^\beta$	−0.63	−0.43	−0.53	−0.15	−0.33	−0.40	−0.28	−0.26
$\Delta\sigma^c$	2.67	1.60	1.11		1.41	1.14	0.76	0.00

[a] The calculated shifts were obtained as an average from four clusters based on geometries from ref 24. [b] Ref 22. [c] Mean absolute deviation.
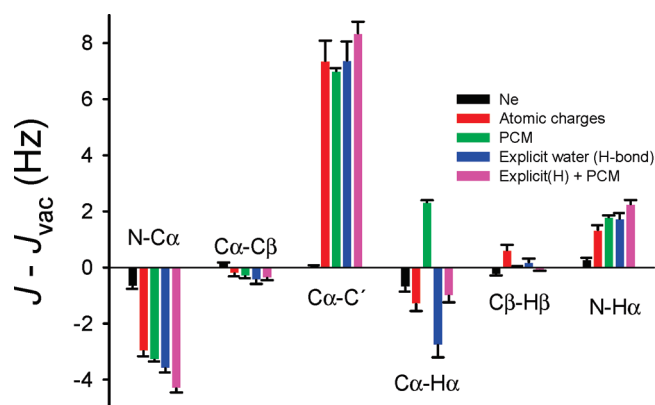
Figure 7. Calculated (B3LYP/6-311++G**) changes of selected AZW J-coupling constants caused by five different solvation models (cf. Figure 6). Cluster results were averaged for four CPMD AZW/H$_2$O geometries.

AZW *J* Coupling. As discussed previously, the indirect spin−spin coupling is a significantly more local property than the chemical shift.[24,36] Consequently, its dependence on the solvent is limited: The polarization neon model (the first in Figure 7) has a minor influence on calculated AZW coupling constants. On the other hand, the lower-level point charge and PCM solvent models provide changes that are all comparable with the most advanced explicit/PCM approximation (Figure 7). However, the PCM model fails for the $J(C^\alpha-H^\alpha)$ constant. This may be an accident, as both the DFT approximation itself and neglecting the vibrational averaging significantly contribute to an overall error of the calculated *J*-coupling constants.[2,24,36,55] In any case, the importance of the solvent for the nonpolar C$^\alpha$−H$^\alpha$ moiety is rather surprising.

On average, the PCM results reasonably well explain the experimental solvent influence on the *J*-coupling constants for the three alanine charged forms, as documented in Table 3, where also other solvent models and the experimental values are listed. Very good solvent correction is obtained also with a computationally cheap atomic partial charge model combined with the PCM environment.

NMR Shielding and Coupling in Nonaqueous Solvents. Further insight into the mechanisms of the solvation effects can be obtained by comparison of more solvents. We plotted the calculated shift and spin−spin coupling constant changes caused in the chloroform molecule by the acetone, acetonitrile, benzene, chloroform, dimethylsulfoxide, and methanol solvents in Figure 8. The NMR parameters were evaluated at the BPW91/6-311++G**(6-31+G* for the solvent) level. The GGA BPW91 functional works approximately as well as B3LYP, but the calculations are significantly faster. As above, we consider the last ("explicit+PCM") model to be the most reliable. Unlike for water (Figures 6 and 7), the replacement of the organic solvents by the partial atomic charges does not provide reliable solvent effects. The carbon chemical shifts obtained with PCM are not realistic, while this approximation gives reasonable hydrogen shifts for some polar solvents (acetone, acetonitrile, and DMSO). The electrostatic (charge and PCM) models particularly fail for benzene; for this molecule, we can observe an exceptionally large NICS "bulk" magnetizability contribution, as can be expected because of its aromatic character. The aromaticity causes the experimentally well-known ring current effects.[32] The aromatic solvent-induced shift (ASIS) has been firstly observed with pyridine and benzene used as solvents and soon systematically was investigated in a series of steroidal compounds.[56] In our case, perhaps surprisingly, the NICS shielding is also important for the chloroform hydrogen solvent shift, where it causes about 80% of the total "explicit + PCM" change.

For the coupling, we defined "NICS" coupling values, in an analogy to the shift, as a coupling constant between two solute nuclei. The nuclei were treated as pseudo(ghost)-atoms, without electrons and a basis set, so that the coupling was enabled by the solvent electrons only. Such coupling thus represents a direct magnetic interaction between the solute nuclei mediated by the solvent. As expected, this effect is rather small (orange bars in the bottom panel in Figure 8) but may become important for more precise computations in the future. According to our knowledge, it has never been estimated before.

296 *J. Chem. Theory Comput.*, Vol. 6, No. 1, 2010

Dračínský and Bouř

Table 3. Calculated and Experimental Indirect Spin–Spin Coupling Constants (Hz) for the Three Alanine Forms

	C^α	vacuum	cluster	point charge	PCM	point charge+PCM	cluster+PCM	exptl.[a]
AZW	$N-C^\alpha$	0.1	−3.5	−2.8	−3.2	−3.4	−4.2	−5.7
	$C^\alpha-C^\beta$	33.6	33.1	33.3	33.2	33.3	33.2	34.9
	$C^\alpha-C'$	45.4	52.8	52.8	52.4	52.9	53.8	54.0
	$C^\alpha-H^\alpha$	142.8	140.0	141.5	145.1	144.4	141.8	145.1
	$C^\beta-H^\beta$	123.4	123.6	124.0	123.4	123.5	123.3	129.7
	$N-H^\alpha$	−3.4	−1.7	−2.1	−1.6	−1.7	−1.2	0.0
	$N-C^\beta$	0.0	−0.1	−0.1	−0.2	−0.2	−0.4	0.0
	$N-C'$	0.1	−0.1	−0.1	−0.1	−0.1	−0.1	0.0
	$C^\alpha-H^\beta$	−2.5	−2.9	−2.8	−2.8	−2.8	−3.0	−4.4
	$C^\beta-H^\alpha$	−2.4	−2.7	−2.7	−3.0	−2.9	−3.0	−4.6
	$C'-C^\beta$	−1.0	−1.1	−1.2	−1.1	−1.2	−1.1	−1.2
	$C'-H^\alpha$	−3.8	−3.6	−3.8	−4.0	−4.0	−3.6	−5.0
	$N-H^\beta$	−3.8	−3.2	−3.6	−3.5	−3.5	−3.0	−3.1
	$C'-H^\beta$	2.9	3.6	3.5	3.5	3.6	3.9	4.2
	$H^\alpha-H^\beta$	5.8	6.2	6.0	6.1	6.1	6.4	7.3
	ΔJ^b	*2.5*	*1.7*	*1.6*	*1.4*	*1.4*	*1.4*	*0.0*
A^+	$N-C^\alpha$	−5.2	−5.9	−6.0	−6.0	−6.2	−6.0	−6.6
	$C^\alpha-C^\beta$	31.5	32.8	32.4	33.3	33.2	33.5	34.1
	$C^\alpha-C'$	63.1	61.6	62.7	62.2	62.4	60.9	59.6
	$C^\alpha-H^\alpha$	141.4	138.1	139.7	143.5	142.8	141.5	146.6
	$C^\beta-H^\beta$	128.1	126.3	127.3	125.7	125.9	125.0	131.0
	$N-H^\alpha$	−1.1	−0.2	−0.6	−0.3	−0.2	0.0	0.0
	$N-C^\beta$	−0.2	−0.2	−0.3	−0.4	−0.4	−0.3	0.0
	$N-C'$	−0.5	−0.7	−0.5	−0.4	−0.4	−0.6	0.0
	$C^\alpha-H^\beta$	−3.0	−3.3	−3.2	−3.3	−3.3	−3.4	−4.6
	$C^\beta-H^\alpha$	−3.8	−3.9	−3.9	−4.1	−4.1	−4.2	−4.9
	$C'-C^\beta$	−1.4	−1.1	−1.2	−1.3	−1.3	−1.1	−1.3
	$C'-H^\alpha$	−6.2	−5.7	−5.9	−6.2	−6.1	−5.8	−6.0
	$N-H^\beta$	−4.1	−3.1	−3.6	−3.5	−3.4	−2.9	−3.0
	$C'-H^\beta$	4.3	4.4	4.4	4.4	4.4	4.5	4.6
	$H^\alpha-H^\beta$	6.5	6.7	6.6	6.5	6.6	6.7	7.3
	ΔJ^b	*1.5*	*1.5*	*1.4*	*1.1*	*1.2*	*1.2*	*0.0*
A^-	$N-C^\alpha$	−3.3	−3.1	−3.5	−2.8	−3.4	−2.8	−4.3
	$C^\alpha-C^\beta$	36.3	35.6	36.2	36.2	35.9	35.5	35.2
	$C^\alpha-C'$	49.6	50.3	50.9	50.4	51.0	50.0	52.7
	$C^\alpha-H^\alpha$	130.5	130.5	130.2	132.9	132.1	131.9	138.4
	$C^\beta-H^\beta$	118.1	120.3	119.7	120.2	121.1	120.9	127.6
	$N-H^\alpha$	−3.4	−2.5	−2.8	−2.7	−2.5	−2.3	−2.2
	$N-C^\beta$	−4.9	−3.3	−3.9	−4.3	−3.6	−0.3	0.0
	$N-C'$	0.9	1.1	1.0	0.9	1.1	1.1	0.0
	$C^\alpha-H^\beta$	−3.0	−3.2	−3.1	−3.2	−3.1	−3.2	−4.3
	$C^\beta-H^\alpha$	−2.9	−3.6	−3.4	−3.4	−3.5	−3.7	−4.7
	$C'-C^\beta$	0.3	0.2	0.3	0.4	0.1	0.2	0.0
	$C'-H^\alpha$	−3.7	−3.1	−3.3	−3.4	−3.3	−3.0	−4.3
	$N-H^\beta$	−3.5	−3.3	−3.5	−3.5	−3.6	−3.3	−3.0
	$C'-H^\beta$	3.1	3.6	3.4	3.6	3.6	3.8	4.3
	$H^\alpha-H^\beta$	6.0	6.3	6.2	6.2	6.2	6.4	7.1
	ΔJ^b	*2.4*	*2.0*	*2.1*	*2.0*	*1.8*	*1.6*	*0.0*

[a] Ref 22. [b] Mean absolute deviation.

Another important difference between the solvated alanine and chloroform is the indifference of the carbon and hydrogen NMR parameters to the addition of the PCM continuum around the explicit cluster. Only for the J(CH) coupling constant in DMSO and methanol solvents does the addition of PCM cause larger changes. This can be explained by the absence of a strong chloroform-solvent hydrogen-bond-like interaction, lower polarity of the organic solvents, and their comparatively larger size (against H_2O). Indeed, as apparent from the radial distribution functions in Figure 9, the used cutoff of 9 Å allows inclusion of most of the orientation effects associated with the arrangement of the solvent in the first solvation sphere. For larger radii, the radial distribution functions (solvent densities) quickly converge to the experimental values (cf. also Table 1), although minor oscillations can still be seen even at larger distances, in particular for DMSO.

DFT Functional and Basis Set Dependence. For control computations, we also estimated the influence of a functional (BPW91 → B3LYP) and basis set applied used for the solvent (6-31+G*→6-311++G**) on the predicted solvent effects in Figure 8. This did not bring significant qualitative changes. For absolute values, however, the basis set change still caused differences up to 0.4 ppm and 0.1 ppm for the carbon and hydrogen chemical shifts and 0.8 Hz for the C−H coupling, for example. The results obtained with the different functionals differed much less (∼0.1 ppm for the shifts and ∼0.2 Hz for the coupling).

Comparison to Experimental Chloroform NMR Spectra. As an ultimate test, the NMR parameters calculated with the MD solvent/chloroform clusters are compared to experimental results. In Figure 10, ^{13}C and ^{1}H chemical shifts (with respect to pure chloroform) are plotted as calculated and

Computational Analysis of Solvent Effects

J. Chem. Theory Comput., Vol. 6, No. 1, 2010 **297**
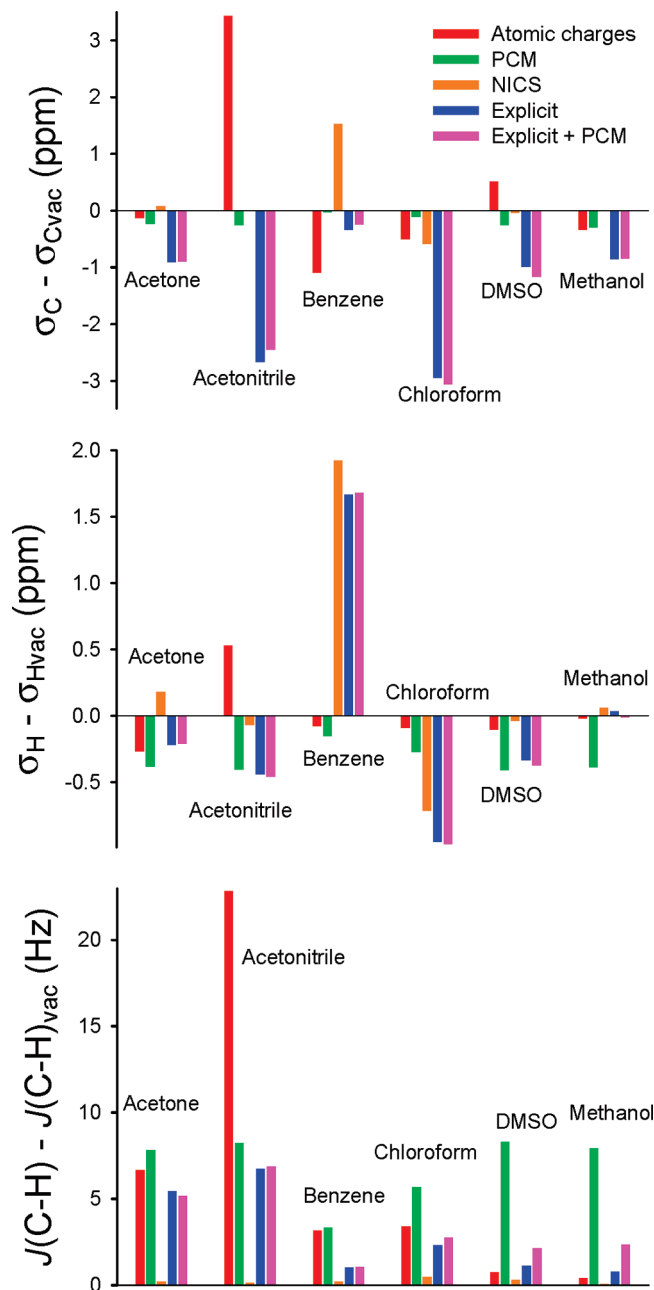

Figure 8. Calculated (BPW91/6-311++G**/6-31+G*) solvent-induced carbon (top) and hydrogen (middle) chemical shifts and changes of the C−H coupling constant (bottom) for chloroform in different solvents. Five solvent approximations were adopted as indicated.
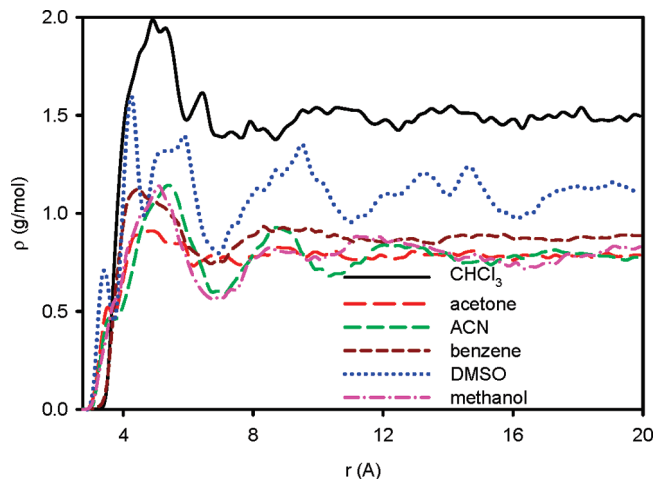

Figure 9. Radial distribution densities of the six solvents surrounding the chloroform molecule obtained by the NVT Amber99 MD simulations. The density was integrated with respect to the CHCl$_3$ carbon atom.

measured for the six solvents. A total of 10 clusters were averaged for each point, and the standard error of the mean is indicated. Overall, the main trends are well-reproduced; the results obtained with the MD solvent clusters could further be improved when the bulk influence was arbitrarily added as 1/3 of the relative magnetic susceptibility (Table 1) for all solvents, mimicking thus a spherical cavity. The BPW91 and B3LYP functionals provide nearly the same results. The calculated solvent effects (the slope in the graphs, compare to the line $y = x$) are overestimated for ^{13}C and underestimated for ^{1}H in comparison with the experiment. Interestingly, the NVT dynamics provided much larger solvent effects than NpT. Such a sensitivity of the NMR

shielding to the MD model has already been observed for the alanine,[24] where the CPMD simulation gave better results than a classical MD. For the larger chloroform/solvent clusters, unfortunately, the CPMD computations take too long.

A very good overall agreement can also be observed between the calculated and experimental solvent changes in the *J*(CH) coupling (Figure 11). Here, the NVT geometries provided somewhat better results than those from the NpT simulation. This can be attributed to more realistic NVT solvent densities; the NpT simulation underestimates both densities and coupling solvent effects. The solvent coupling effect on *J*(CH) seems to be primarily driven by the polarity of the solvent. The DMSO induces the biggest changes with respect to the nonpolar solvents, but the dependence does not follow the electric permittivity for similarly polar solvents blindly (the respective permittivities for CHCl$_3$, C$_6$H$_6$, CD$_3$CN, MeOH, acetone, and DMSO are ε_r = 4.7, 2.3, 35.7, 32.6, 20.5, and 46.9). The good agreement with the experiment and the variation of the results with the MD parameters also indicate desirable improvements in future simulations of the NMR parameters. Inevitably, solvent and solute molecular dynamics have to become more reproducible.

4. Conclusions

On several models, we have investigated various factors that are important for an understanding and reliable modeling of the solvent effects on NMR chemical shifts and indirect spin−spin coupling constants. In spite of the complexity, such as the delocalized character of the magnetic phenomena, the cluster models, where the geometry is derived from relatively accurate MD simulations and properly averaged over a modest number of configurations, recover the most important changes observed for the NMR parameters in the experiment. Needless to say, ab initio molecular dynamics, when possible, provide more reliable results than empirical MD force fields.

For the shielding, a correct description of the solvent orientation in the first solvation sphere appeared particularly
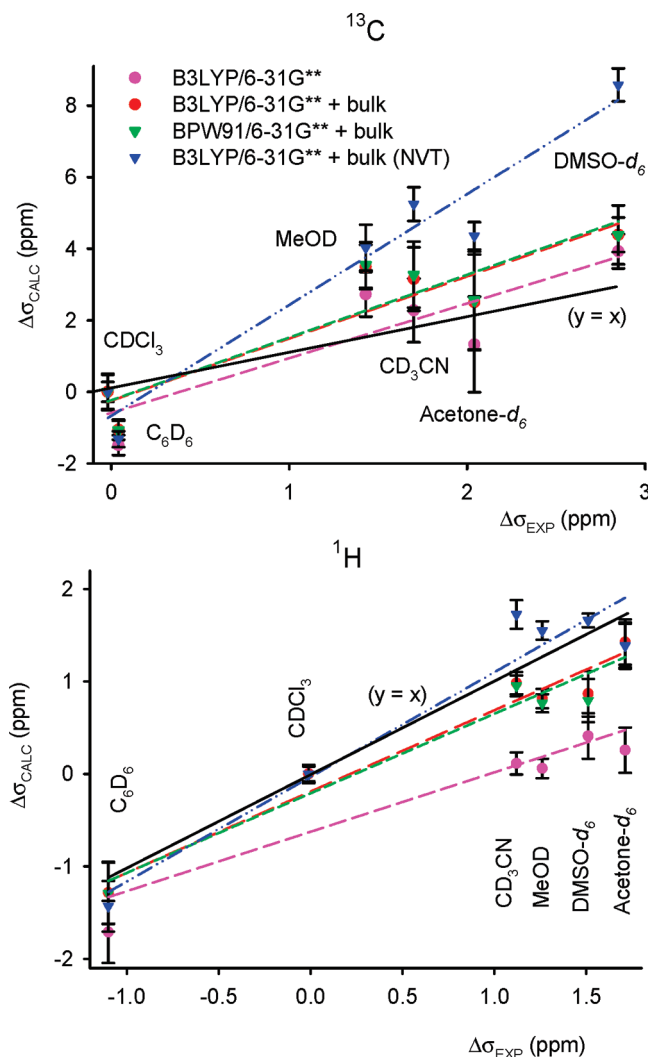
Figure 10. Experimental versus calculated ^{13}C (top) and ^1H (bottom) chemical shifts of chloroform in various solvents, referenced to pure $CHCl_3$. The calculated solvent shifts were obtained as averages of 10 independent MD geometries. By default, the NpT thermodynamic ensemble was used. Errors of the means are indicated.
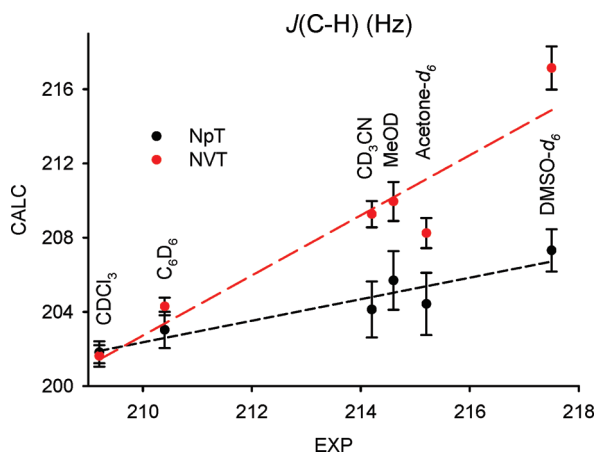

Figure 11. Correlation of experimental and calculated (B3LYP/6-31G**) chloroform C–H coupling constants in various solvents. For results obtained as averages of 10 random clusters from NpT or NVT MD simulations, the errors of the mean are indicated.

crucial for precise results. The far-ranging bulk influence could be estimated only roughly from computations on large clusters or from the solvent magnetic susceptibility. The isotropic shielding was found to be very sensitive to specific solvent−solute interactions and solvent orientation in the hydration spheres.

The indirect spin−spin coupling behaved as a much more local phenomenon than the shielding. The solvent effects, primarily dependent on electrostatic interactions, could be modeled at a relatively low level of approximation, for example, with the atomic partial charges or a polarizable continuum.

The modeling provided chemical shifts and indirect spin−spin coupling constants for the alanine charged forms that compared well with the previous experimental results. Similarly for the chloroform NMR data, the calculated results reasonably well explained differences observed experimentally for six organic solvents. The calculated results were strongly dependent on the adopted molecular dynamics model. Nevertheless, the modeling revealed the large potential of the NMR spectroscopy to study not only molecular structure and conformation, but also the specific solvent−solute interactions and structures of the solvation shells.

References

(1) Evans, J. N. S. *Biomolecular NMR Spectroscopy*; Oxford University Press: Oxford, U. K., 1995.

(2) Kaupp, M.; Bühl, M.; Malkin, V. G. *Calculation of NMR and EPR Parameters: Theory and Applications*; Wiley-VCH: Weinheim, Germany, 2004.

(3) Otting, G.; Liepinsh, E. *Acc. Chem. Res.* **1995**, *28*, 171.

(4) Ditchfield, R. *Mol. Phys.* **1974**, *27*, 789.

(5) Cheeseman, J. R.; Trucks, G. W.; Keith, T.; Frisch, M. J. *J. Chem. Phys.* **1996**, *104*, 5497.

(6) Sychrovský, V.; Gräfenstein, J.; Cremer, D. *J. Chem. Phys.* **2000**, *113*, 3530.

(7) Luhmer, M.; Bartik, K. *J. Phys. Chem. A* **1997**, *101*, 5278.

(8) Cossi, M.; Rega, N.; Scalmani, G.; Barone, V. *J. Comput. Chem.* **2002**, *24*, 669.

(9) Caricato, M.; Ingrosso, F.; Mennucci, B.; Tomasi, J. *J. Chem. Phys.* **2005**, *122*, 154501.

(10) Cossi, M.; Barone, V. *J. Chem. Phys.* **1998**, *109*, 6246.

(11) Jalkanen, K. J.; Nieminen, R. M.; Frimand, K.; Bohr, J.; Bohr, H.; Wade, R. C.; Tajkhorshid, E.; Suhai, S. *Chem. Phys.* **2001**, *265*, 125.

(12) Bouř, P.; Michalík, D.; Kapitán, J. *J. Chem. Phys.* **2005**, *122*, 144501.

(13) Bouř, P. *J. Chem. Phys.* **2004**, *121*, 7545.

(14) Bouř, P.; Keiderling, T. A. *J. Chem. Phys.* **2003**, *119*, 11253.

Computational Analysis of Solvent Effects

J. Chem. Theory Comput., Vol. 6, No. 1, 2010 **299**

(15) Ebrahimi, A.; Habibi, M.; Masoodi, H. R. *Chem. Phys. Lett.* **2009**, *478*, 120.

(16) Cammi, R.; Mennucci, B.; Tomasi, J. *J. Phys. Chem. A* **2000**, 104.

(17) Caricato, M.; Mennucci, B.; Tomasi, J.; Ingrosso, F.; Cammi, R.; Corni, S.; Scalmani, G. *J. Chem. Phys.* **2006**, *124*, 124520.

(18) Šebek, J.; Kejík, Z.; Bouř, P. *J. Phys. Chem. A* **2006**, *110*, 4702.

(19) Šebek, J.; Bouř, P. *J. Phys. Chem. A* **2008**, *112*, 2920.

(20) Šebek, J.; Gyurscik, B.; Šebestík, J.; Kejík, Z.; Bernárová, L.; Bouř, P. *J. Phys. Chem. A* **2007**, *111*, 2750.

(21) Ruud, K.; Åstrand, P. O.; Taylor, P. R. *J. Am. Chem. Soc.* **2001**, *123*, 4826.

(22) Sychrovský, V.; Buděšínský, M.; Benda, L.; Špirko, V.; Vokáčová, Z.; Šebestík, J.; Bouř, P. *J. Phys. Chem. B* **2008**, *112*, 1796.

(23) Bouř, P.; Buděšínský, M.; Špirko, V.; Kapitán, J.; Šebestík, J.; Sychrovský, V. *J. Am. Chem. Soc.* **2005**, *127*, 17079.

(24) Dračínský, M.; Kaminský, J.; Bouř, P. *J. Phys. Chem. B* **2009**, *113*, 16698.

(25) Woodford, J. N.; Harbison, G. S. *J. Chem. Theory Comput.* **2006**, *2*, 1464.

(26) Kongsted, J.; Nielsen, C. B.; Mikkelsen, K. V.; Christiansen, O.; Ruud, K. *J. Chem. Phys.* **2007**, *126*, 034510.

(27) Aidas, K.; Møgelhøj, A.; Kjær, H.; Nielsen, C. B.; Mikkelsen, K. V.; Ruud, K.; Christiansen, O.; Kongsted, J. *J. Phys. Chem. A* **2007**, *111*, 4199.

(28) Autschbach, J.; Ziegler, T. *J. Am. Chem. Soc.* **2001**, *123*, 3341.

(29) Buehl, M.; Golubnychiy, V. *Magn. Reson. Chem.* **2008**, *46*, S36.

(30) Watts, V. S.; Goldstein, J. H. *J. Phys. Chem.* **1966**, *70*, 3887.

(31) Hoffman, R. E. *J. Magn. Reson.* **2003**, *163*, 325.

(32) Gomes, J. A. N. F.; Mallion, R. B. *Chem. Rev.* **2001**, *101*, 1349.

(33) Hoffman, R. E. *J. Magn. Reson.* **2006**, *178*, 237.

(34) Kümmel, S.; Kronik, L.; Perdew, J. P. *Phys. Rev. Lett.* **2004**, *93*, 213002.

(35) Vignale, G.; Rasolt, M. *Phys. Rev. B* **1988**, *37*, 10685.

(36) Dračínský, M.; Kaminský, J.; Bouř, P. *J. Phys. Chem.* **2009**, *130*, 094106.

(37) Horák, Z.; Krupka, F. *Fyzika*; SNTL: Praha, Czech Republic, 1981.

(38) Ponder, J. W. *Tinker, Software Tools for Molecular Design, 3.8*; Washington University School of Medicine: Saint Louis, MO, 2000.

(39) Wang, J.; Cieplak, P.; Kollman, P. A. *J. Comput. Chem.* **2000**, *21*, 1049.

(40) Jorgensen, W. L.; Chandrasekhar, J.; Madura, J. D. *J. Chem. Phys.* **1983**, *79*, 926.

(41) Asher, J. R.; Doltsinis, N. L.; Kaupp, M. *Magn. Reson. Chem.* **2005**, *43*, S237.

(42) Becke, A. D. *J. Chem. Phys.* **1993**, *98*, 5648.

(43) Vanderbilt, D. *Phys. Rev. B* **1990**, *41*, 7892.

(44) Car, R.; Parrinello, M. *Phys. Rev. Lett.* **1985**, 55.

(45) Lii, J. H.; Allinger, N. L. *J. Comput. Chem.* **1998**, *19*, 1001.

(46) Bouř, P.; Keiderling, T. A. *J. Chem. Phys.* **2002**, *117*, 4126.

(47) Bouř, P. *Collect. Czech. Chem. Commun.* **2005**, *70*, 1315.

(48) Becke, A. *Phys. Rev. A* **1988**, *38*, 3098–3100.

(49) Mennucci, B.; Cancès, E.; Tomasi, J. *J. Phys. Chem. B* **1997**, *101*, 10506.

(50) Besler, B. H.; Merz, K. M.; Kollman, P. A. *J. Comput. Chem.* **1990**, *11*, 431.

(51) Chen, Z.; Corminboeuf, C.; Heine, T.; Bohmann, J.; Schleyer, P. R. *J. Am. Chem. Soc.* **2003**, *125*, 13930.

(52) Frisch, M. J.; Trucks, G. W.; Schlegel, H. B.; Scuseria, G. E.; Robb, M. A.; Cheeseman, J. R.; Montgomery, J. A., Jr.; Vreven, T.; Kudin, K. N.; Burant, J. C.; Millam, J. M.; Iyengar, S. S.; Tomasi, J.; Barone, V.; Mennucci, B.; Cossi, M.; Scalmani, G.; Rega, N.; Petersson, G. A.; Nakatsuji, H.; Hada, M.; Ehara, M.; Toyota, K.; Fukuda, R.; Hasegawa, J.; Ishida, M.; Nakajima, T.; Honda, Y.; Kitao, O.; Nakai, H.; Klene, M.; Li, X.; Knox, J. E.; Hratchian, H. P.; Cross, J. B.; Bakken, V.; Adamo, C.; Jaramillo, J.; Gomperts, R.; Stratmann, R. E.; Yazyev, O.; Austin, A. J.; Cammi, R.; Pomelli, C.; Ochterski, J. W.; Ayala, P. Y.; Morokuma, K.; Voth, G. A.; Salvador, P.; Dannenberg, J. J.; Zakrzewski, V. G.; Dapprich, S.; Daniels, A. D.; Strain, M. C.; Farkas, O.; Malick, D. K.; Rabuck, A. D.; Raghavachari, K.; Foresman, J. B.; Ortiz, J. V.; Cui, Q.; Baboul, A. G.; Clifford, S.; Cioslowski, J.; Stefanov, B. B.; Liu, G.; Liashenko, A.; Piskorz, P.; Komaromi, I.; Martin, R. L.; Fox, D. J.; Keith, T.; Al-Laham, M. A.; Peng, C. Y.; Nanayakkara, A.; Challacombe, M.; Gill, P. M. W.; Johnson, B.; Chen, W.; Wong, M. W.; Gonzalez, C.; Pople, J. A. *Gaussian 03*, revision C.02; Gaussian, Inc.: Wallingford, CT, 2004.

(53) Bouř, P.; Raich, I.; Kaminský, J.; Hrabal, R.; Čejka, J.; Sychrovský, V. *J. Phys. Chem. A* **2004**, *108*, 6365.

(54) DeCamp, M. F.; DeFlores, L.; McCracken, J. M.; Tokmakoff, A.; Kwac, K.; Cho, M. *J. Phys. Chem. B* **2005**, *2005*, 11016.

(55) Ruden, T. A.; Lutnaes, O. B.; Helgaker, T.; Ruud, K. *J. Chem. Phys.* **2003**, *118*, 9572.

(56) Laszlo, P. *Prog. NMR Spectrosc.* **1967**, *3*, 231.

CT900498B